Biosensors and Bioelectronics 77 (2016) 740–745

Contents lists available at ScienceDirect

Biosensors and Bioelectronics

journal homepage: www.elsevier.com/locate/bios

Intense charge transfer surface based on graphene and thymine–Hg (II)–thymine base pairs for detection of Hg^{2+}

Jiao Li, Liping Lu*, Tianfang Kang, Shuiyuan Cheng

Key Laboratory of Beijing on Regional Air Pollution Control, Beijing University of Technology, Beijing 100124, China

ARTICLE INFO

Article history:
Received 3 July 2015
Received in revised form
10 October 2015
Accepted 14 October 2015
Available online 22 October 2015

Keywords:
Biosensor
Hg(II)
DNA charge transfer
Electrochemiluminescence
Quantum dots
Graphene

ABSTRACT

In this article, we developed an electrochemiluminescence (ECL) sensor with a high-intensity charge transfer interface for Hg^{2+} detection based on Hg(II)-induced DNA hybridization. The sensor was fabricated by the following simple method. First, graphene oxide (GO) was electrochemically reduced onto a glassy carbon electrode through cyclic voltammetry. Then, amino-labeled double-stranded (ds)DNA was assembled on the electrode surface using 1-pyrenebutyric acid N-hydroxysuccinimide as a linker between GO and DNA. The other terminal of dsDNA, which was labeled with biotin, was linked to CdSe quantum dots *via* biotin–avidin interactions. Reduced graphene oxide has excellent electrical conductivity. dsDNA with T–Hg(II)–T base pairs exhibited more facile charge transfer. They both accelerate the electron transfer performance and sensitivity of the sensor. The increased ECL signals were logarithmically linear with the concentration of Hg(II) when Hg^{2+} was present in the detection solution. The linear range of the sensor was 10^{-11} to 10^{-8} mol/L (R=0.9819) with a detection limit of 10^{-11} mol/L. This biosensor exhibited satisfactory results when it was used to detect Hg(II) in real water samples. The biosensor with high-intense charge transfer performance is a prospect avenue to pursue more and more sensitive detection method.

1. Introduction

Heavy metal ion-based pollution has become a critical issue worldwide. Particularly, mercury is a highly toxic heavy metal that can greatly harm human health (Niu et al., 2011; Li et al., 2011). Moreover, Hg(II) is difficult to biodegrade, so it can accumulate in organisms through conversion into methyl mercury, which causes various human diseases such as brain damage, kidney failure, and cognitive and motion disorders (Jiang and Wang, 2009). Therefore, it is of great importance to develop a rapid and eco-friendly method to detect Hg(II) with high sensitivity and selectivity. Over the past few years, numerous methods to detect Hg(II) have been developed, such as inductively coupled plasma mass spectrometry (ICP-MS) (Louie et al., 2012), atomic fluorescence spectroscopy (Reis et al., 2014), atomic absorption spectroscopy (Escudero et al., 2013), fluorescent spectrophotometry (Tan et al., 2011), and X-ray absorption spectroscopy (George et al., 2010). However, these traditional methods have disadvantages like complicated sample preparation, large sample volume, and complex instruments (Niu et al., 2011). To overcome these drawbacks, great efforts to analyze Hg(II) have been made using methods such as electrochemistry (Zhao and Zhou, 2012) and electrochemiluminescence (ECL) (Huang et al., 2013; Gao et al., 2013). Specially, ECL has not only simple and controllable electrochemistry but also allows sensitive optical analysis. In addition, compared with fluorescence, ECL has low background signal.

In order to improve the sensitivity of sensor, different kinds of methods have been used, such as catalysis, circulation amplification and increased electrode area. Here, we designed a high-intensity electron transfer interface to obtain highly sensitive detection of Hg(II). Firstly, it is well-known that nanomaterials have been used to increase electron transfer of sensors. Among the various nanomaterials, graphene has attracted extensive attention because of its remarkable physicochemical properties including excellent thermal and electrical conductivities, large surface area, good biocompatibility and high mechanical strength. These unique physicochemical properties suggest that graphene has great potential for providing new approaches and improvements in the field of sensors. For example, the high surface area of graphene can afford an ultrahigh loading capacity for analytical molecules. This in turn can improve sensitivity and allow device miniaturization. Moreover, rapid heterogeneous electron transfer between graphene and redox species open up opportunities to facilitate electron transfer in electrochemical systems.

Meanwhile, we noticed another attracting approach for higher charge transfer performance. Ono and co-workers reported that

* Corresponding author.
E-mail address: lipinglu@bjut.edu.cn (L. Lu).

http://dx.doi.org/10.1016/j.bios.2015.10.047
0956-5663/

thymine–thymine (T–T) base pair mismatches could selectively capture Hg^{2+} to form T–Hg(II)–T base pairs in 2006 (Zhang et al., 2013; Ma et al., 2013). This property allowed Hg(II) detection with high selectivity even in the presence of related environmental heavy metal ions. A series of Hg^{2+} biosensors based on T–Hg(II)–T were then developed that used approaches including fluorescence (Wang et al., 2014), electrochemistry (Xu et al., 2015), and quartz crystal microbalance (Dong and Zhao, 2012). The T–Hg(II)–T complex is even more stable than the Watson–Crick adenine-T base pair (Zhang and Guo, 2012) and accelerates the rate of charge transfer in DNA (Kratochviova et al., 2014).

Thus, based on the high electron transfer rate of graphene and charge transfer rate of T–Hg(II)–T, we designed a DNA ECL biosensor for Hg(II) detection based on a high-intensity charge transfer surface. Using a specific T-rich double-stranded (ds) DNA, the ECL intensity of the biosensor increases with Hg(II) concentration. The proposed biosensor is used to detect Hg(II) in real water samples with high sensitivity and good selectivity.

2. Experimental sections

2.1. Chemicals and materials

$CdCl_2 \cdot 2.5H_2O$ and $K_2S_2O_8$ were purchased from Beijing Chemical Reagent Corporation. Selenium was purchased from Shanghai Meixing Chemical Corporation. Mercaptopropionic acid, avidin (from egg white), 1-pyrenebutyric acid N-hydroxy-succinimide ester (PASE), ethanolamine, N,N-dimethylformamide (DMF), 1-(3-dimethylaminopropyl)-3-ethylcarbodiimide hydrochloride and hexaammineruthenium(III) chloride were purchased from Sigma-Aldrich (USA). $NaBH_4$, $Na_2HPO_4 \cdot 12H_2O$, $NaH_2PO_4 \cdot 2H_2O$, KCl, $HgCl_2$, $FeCl_3 \cdot 6H_2O$, $FeCl_2 \cdot 4H_2O$, $MnCl_2 \cdot 4H_2O$, $CuCl_2$, NaCl, $AlCl_3$, $PbCl_2$, $CrCl_3$, $BaCl_2$, AgCl and $CaCl_2$ were purchased from Tianjin Fuchen Chemical Corporation. $MgCl_2$ was purchased from Shanghai Sangon Biotechnology Corporation. N-Hydroxysuccinimide was purchased from Sinopharm Chemical Reagent Limited Corporation. Graphene oxide (GO) dispersion (2 mg/mL, dispersed in water) was purchased from Nanjing XFNANO Materials Technology Corporation. All reagents were analytical grade. Ultrapure water prepared by a Milli-Q system (Millpore, USA) was used in all experiments.

Four labeled single-stranded oligonucleotides (ss-DNA) in the experiments were synthesized by Shanghai Sangon Biotechnology Corporation (Shanghai,China). The sequences of the four ss-DNA used in this work were:

ssDNA-1: 5′-NH_2-CGC GCG CTT TTT TTT TT-3′
ssDNA-2: 5′-biotin-TTT TTT TTT TGC GCG CG-3′
ssDNA-3: 5′-NH_2-CAT GCA TGC ATG CAT GC-3′
ssDNA-4: 5′-biotin-GCA TGC ATG CAT GCA TG-3′

All the double-stranded DNA were obtained by hybridization of single stranded DNA. dsDNA-1 was obtained by mixing ssDNA-1 and ssDNA-2 with the same molar ratio and then incubation at 90 °C for 5 min before cooling slowly to room temperature. The dsDNA-2 was formed by hybridization of ssDNA-3 and ssDNA-4 using the process described above, which was only used to determine the electron transfer rate of normal dsDNA. The dsDNA-1 was used in all the other experiments.

Electrochemical impedance spectroscopy (EIS) and cyclic voltammetry (CV) were carried out on a CHI 660 a electrochemical workstation (Shanghai Chenhua Instrument Corporation). ECL was detected using a MPI-A ECL analyzer (Xi'an Remex Analysis Instrument Corporation). All experiments were performed using a three-electrode system with a platinum wire as the counter electrode, sensor as the working electrode and Ag–AgCl electrode (saturated KCl) as the reference electrode. Field-emission scanning electron microscopy (SEM) was conducted with a 2100F microscope (JEOL). UV–vis absorption spectra were recorded on a UV-2450 spectrophotometer (Shimadzu). Fluorescence spectra were obtained on an F-4600 fluorescence spectrophotometer (Hitachi). ICP-MS detection was performed on a 7700 Series spectrometer (Agilent Technologies).

2.2. Pretreatment of a glassy carbon electrode (GCE)

Prior to use, a GCE was polished carefully with an aqueous 0.05-μm Al_2O_3 suspension, and then sonicated adequately in ultrapure water, ethanol and ultrapure water in turn. The electrode was immersed in 0.5 mol/L H_2SO_4 for a CV scan in a potential range of −0.3 to 1.5 V. The treated GCE was rinsed thoroughly with ultrapure water and dried with pure N_2.

2.3. Electrodeposition of GO on a GCE

GO was directly deposited onto a GCE through CV reduction in GO dispersion (1 mg/mL) with gentle magnetic stirring and N_2 bubbling (Yang et al., 2013; Chen et al., 2011). The CV potential range was 0.5 to −1.5 V and the scan rate was 100 mV/s. After electrodeposition, the electrode was thoroughly washed with 0.1 mol/L phosphate-buffered saline (PBS; 0.1 mol/L $HPO_4^{2-}/H_2PO_4^-$, 0.1 mol/L KCl, pH 7.4) and dried with N_2. In this process, GO formed electroreduced GO (ERGO); this electrode is denoted as ERGO/GCE.

2.4. Immobilization of dsDNA on the ERGO/GCE (Du et al., 2013)

The ERGO/GCE was immersed in a solution of PASE in DMF for 1 h, then washed sufficiently with DMF and water, and dried under an N_2 flow. The electrode was incubated in a 50 μmol/L dsDNA solution for 2 h at room temperature. The electrode was backfilled with 100 mmol/L ethanolamine (pH 9.0) for 30 min and then thoroughly rinsed with 0.1 mol/L PBS. After drying under an N_2 flow, the dsDNA/ERGO/GCE was obtained. Here, PASE was used as a linker to immobilize dsDNA because it can covalently bind with an amino-terminated dsDNA by formation of an amide bond and also firmly attach to the surface of ERGO through π–π stacking with its pyrene group.

2.5. CdSe quantum dots (QDs) as an ECL indicator on the electrode surface

CdSe QDs were synthesized according to the literature (Jiang and Ju, 2007). The CdSe QDs were labeled with avidin by mixing CdSe QDs and avidin in a certain proportion (Stanisavljevic et al., 2013) and centrifuging the mixture at 13,000 rpm for 80 min. The dsDNA/ERGO/GCE was soaked in a solution of avidin-labeled CdSe QDs under shock conditions for 1 h to assemble avidin-labeled CdSe QDs on the dsDNA/ERGO/GCE through formation of biotin-avidin complexes because one terminal of each dsDNA was labeled with biotin. The resulting electrode (denoted CdSe QDs/dsDNA/ERGO/GCE) was rinsed thoroughly with 0.1 mol/L PBS. The fabrication process of the sensor is illustrated in Fig. 1.

2.6. Detection of Hg^{2+}

To detect Hg(II), the CdSe QDs/dsDNA/ERGO/GCE was incubated in $HgCl_2$ solution for 40 min at 37 °C, and then washed with 0.1 mol/L PBS solution. The measurement of Hg(II) was conducted on a MPI-A ECL analyzer with a potential range of −1.5–0 V at a scan rate of 100 mV/s. Before and after incubation in Hg^{2+}

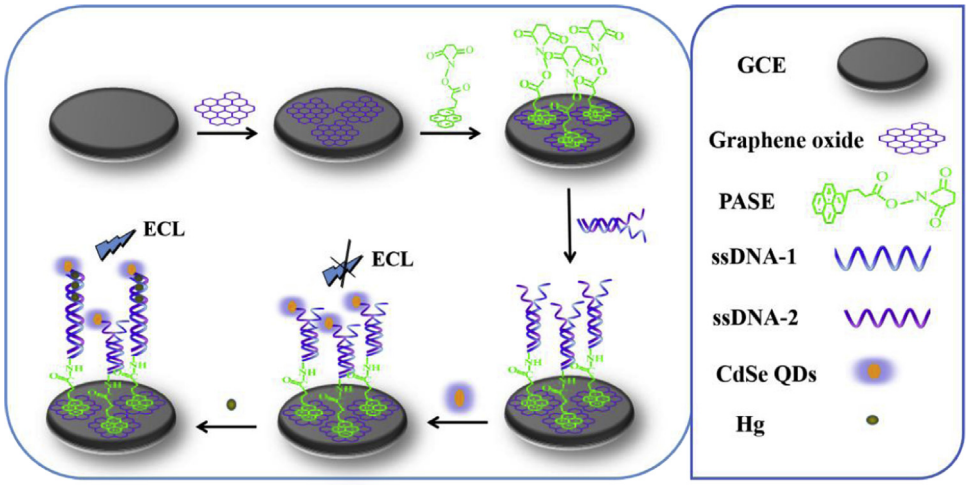

Fig. 1. Scheme of a DNA ECL biosensor and its detection of Hg(II).

solution, the ECL intensity of the sensor was recorded in 0.1 mol/L $K_2S_2O_8$.

3. Results and discussion

3.1. Electrodeposition of GO

Graphene and graphene derivatives have been used in electrochemical sensors to improve their performance. In most cases, graphene has been immobilized on the electrode *via* drop-casting (Filik et al., 2013; Wang and Zhao, 2011). The adsorption method is a simple and quick alternative, but it might be less reproducible than drop-casting, and also has the drawback of lacking control over the graphene film thickness. Therefore, in this article, GO was electrochemically reduced onto GCE to obtain an ERGO film. Moreover, the film thickness could be controlled by changing the number of deposition cycles, and the graphene coating was very stable because of its poor solubility in common solvents (Guo et al., 2009; Zhou et al., 2009; Shao et al., 2010). Fig. 2. shows the process of electrochemical reduction of GO, in which a peak at −1.3 V caused by the reduction of GO on the surface of the electrode was observed. The peak currents tended to gradually stabilize during continuous CV scanning.

The formation of a graphene film on the electrode was directly confirmed by SEM, as shown in the inset of Fig. 2. X-ray photoelectron spectroscopy (data not shown) indicated that the O/C ratio decreased from 0.42 to 0.19 after the GO was electrochemically reduced, implying that GO has been deoxygenated in the ERGO film.

3.2. Quantitation of dsDNA on the GCE electrode

Examination of the surface coverage of DNA confirmed that the high surface area of graphene afforded a high loading capacity for DNA. The surface coverage of dsDNA on the electrode was calculated by Tarlov et al. (Steel et al., 1998) based on the electrochemical response of $Ru(NH_3)_6^{3+}$ (RuHex) electrostatically bound to the dsDNA. We used a chronocoulometry method to determine the redox capacitive charge in 5 mmol/L PBS solution with or without RuHex (100 μmol/L). The density of DNA on the electrode surface was calculated using the following equation:

$$\Gamma_{DNA} = \frac{Q}{nFA}\frac{z}{m}N_A, \quad (1)$$

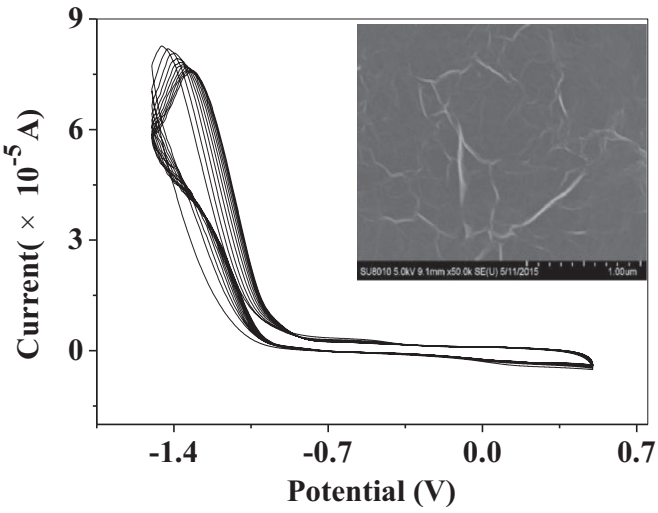

Fig. 2. CVs of the electrochemical reduction of GO. Inset is an SEM image of ERGO.

where Γ_{DNA} is the surface coverage of DNA (mol/cm^2), Q is the capacitive charge (C), n is the number of electrons per redox event, m is the base number of dsDNA, z is the charge number, A is the electrode area (cm^2), and F is the Faraday constant (C/equiv). Fig. S1 depicts the chronocoulometric response curves of dsDNA/GCE. According to Eq. (1), the density of dsDNA on the ERGO surface was about 11.7 pmol/cm^2, which was higher than that of the other surface (~7.4 pmol/cm^2) (Yu et al., 2003).

3.3. Electron transfer rate of dsDNA

Ono's group demonstrated that a T–T mismatch base pair in a DNA duplex can capture an Hg(II) ion to form a stable neutral T–Hg(II)–T base pair (Miyake et al., 2006). We compared the charge transfer rates of standard DNA and DNA with T–Hg(II)–T using an electrochemical technique. Graphene and GO have been reported to interact strongly with nucleic acids through π–π stacking interactions between the ring structures in the base pairs of the nucleic acids and those of graphene and GO (Lu et al., 2009; Jang et al., 2010). In contrast, dsDNA cannot be stably adsorbed onto the surface of graphene because of efficient shielding of the nucleobases within the negatively charged dsDNA phosphate backbone. Moreover, the GO interface can remove the nonspecific adsorption of dsDNA. GO causes the dsDNA to stand on the GO surface and facilitates evaluation of charge transfer.

The rate constant of electron transfer k in DNA on the surface of ERGO was evaluated using the classical model proposed by Laviron and co-workers (Laviron., 1979). First, the dsDNA/ERGO/GCE was immersed in an electrolyte of low ionic strength containing RuHex (1 mmol). We used CV to record the redox potential of RuHex at different scan rates in 5 mmol/L PBS. Then, k was determined using Eq. (2):

$$E_{pc} = E^{0'} - \frac{RT}{\alpha nF} \ln\left(\frac{\alpha nF}{RTk}\right) \quad (2)$$

where E_{pc} is the reduction potential, $E^{0'}$ is the formal potential of RuHex, and α, R, and T are all constants that have their usual meanings.

We calculated k of dsDNA-2/ERGO/GCE and Hg^{2+}/dsDNA/ERGO/GCE, as shown in Fig. S2. k of dsDNA-2/ERGO/GCE was about 2.0 s^{-1} (Pheeney and Barton, 2013), while that of Hg^{2+}/dsDNA/ERGO/GCE reached approximately 3.3 s^{-1}. These results indicate that the DNA with T–Hg(II)–T has a higher rate of charge transfer than the standard DNA duplex. Perturbation of π stacking is important in the charge transfer processes in DNA. Therefore, the local geometry (overlap of the bases) of DNA with T–Hg(II)–T was more favorable for charge transfer than the dsDNA without Hg(II) (Kratochviova et al., 2014).

3.4. Impedance analysis

Electrical conductivity is perhaps the best indicator of the extent to which graphite oxide has been reduced to graphene. EIS can provide information about interfacial charge transfer. In a typical EIS measurements, the semicircle observed at higher frequency corresponds to the charge transfer-limited process and an increase of the diameter of the semicircle reflects an increase of the interfacial resistance to charge transfer (R_{ct}) (Long et al., 2003). Fig. 3(A) illustrates the EIS of the modified GCE at different stages. R_{ct} of ERGO/GCE was obviously lower than that of the bare GCE, which was attributed to the good conductivity of ERGO. GO has poor conductivity, whereas graphene is a good conductor. Therefore, the decrease of R_{ct} indicated that GO was electrochemically reduced and a considerable number of oxide groups were removed from GO to form ERGO. When dsDNA-1 was assembled on the ERGO/GCE, the diameter of the semicircle increased markedly because of the effective repulsion between the negatively charged DNA phosphate backbones and $[Fe(CN)_6]^{3-/4-}$ anions, indicating that the probe NH_2-dsDNA had been grafted on ERGO. After immobilization of CdSe QDs on the dsDNA-1/ERGO/GCE, R_{ct} was further increased. This was attributed to the repulsion between the negatively charged CdSe QDs and $[Fe(CN)_6]^{3-/4-}$ anions. Subsequent incubation in Hg^{2+} solution caused R_{ct} to decrease, indicating that hybridization of T–T mismatched DNA and the formation of dsDNA with T–Hg(II)–T could increase k. These results were consistent with the calculated values of k.

The corresponding CV curves in $[Fe(CN)_6]^{3-/4-}$ were also measured to further determine the surface properties of the electrodes in different stages of modification. Fig. 3(B) reveals that the good conductivity of ERGO causes the current of ERGO/GCE to be greater than that of the bare GCE. The current of dsDNA-1/ERGO/GCE is obviously lower than that of ERGO/GCE. This is mainly attributed to the phosphate backbones of DNA, which carry negative charge, preventing $[Fe(CN)_6]^{3-/4-}$ molecules from reaching electrode surface. In addition, the CdSe QDs are negatively charged, which further decreases the electrode current. However, the presence of Hg^{2+} in the solution caused the current to quickly increase, which is attributed to T–Hg^{2+}–T facilitating charge transfer.

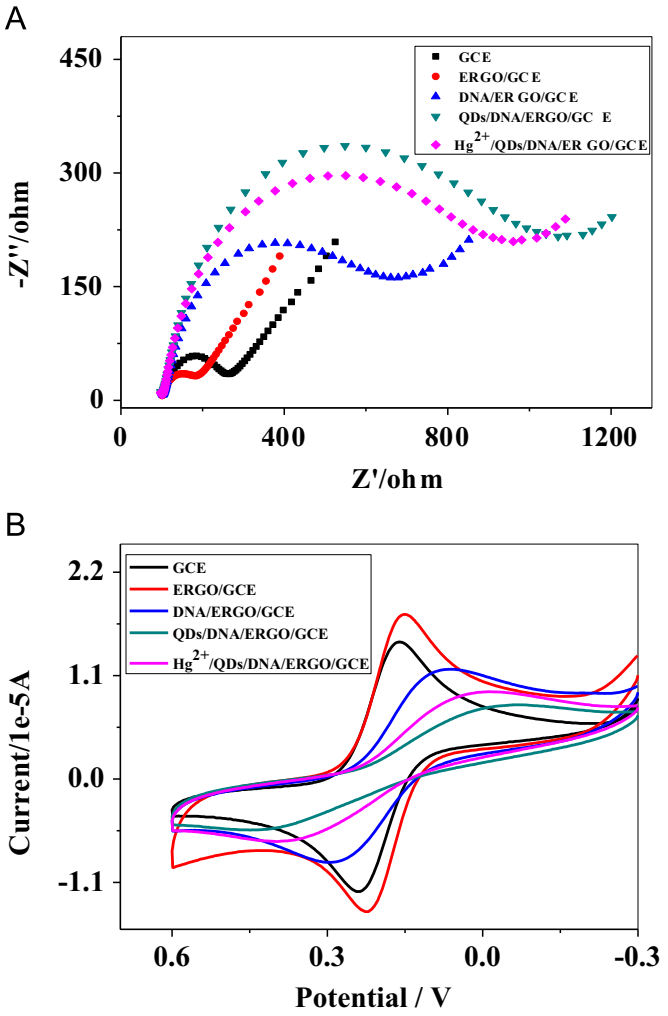

Fig. 3. (A) EIS and (B) CV measurements of modified electrodes.

From the above analysis, we can conclude that the presence of ERGO and dsDNA with T–Hg–T endowed the developed sensor with high-intensity charge transfer.

3.5. Quantitative determination of Hg^{2+}

Fig. 4(A) shows the ECL intensity of the sensor for the detection of different concentrations of Hg^{2+}, while Fig. 4(B) depicts the relationship between ECL intensity and Hg^{2+} concentration. The ECL intensity gradually increased with the addition of Hg^{2+}. This increase of ECL intensity is attributed to the formation of T–Hg(II)–T base pairs, which enhance the rate of electron transfer. The ECL intensity was proportional to the logarithm of Hg^{2+} concentration within the range of 10^{-11}–10^{-8} mol/L (R=0.9819) with a detection limit of 10^{-11} mol/L.

3.6. Selectivity, stability and reproducibility of the sensor

The selectivity of the sensor was evaluated by measuring its ECL signal in the presence of other metal ions including K^+, Ca^{2+}, Na^+, Mg^{2+}, Al^{3+}, Fe^{2+}, Fe^{3+}, Mn^{2+}, Pb^{2+}, Cu^{2+}, Cr^{3+}, Cd^{2+}, Ba^{2+}, and Ag^+. The concentrations of interfering metal ions were 10^{-8} mol/L, which was 10 times higher than that of Hg^{2+}. Fig. 5 reveals that the ECL signals of the sensor incubated with the interfering metal ions were negligible compared with that of the sensor incubated with Hg^{2+}. Therefore, the sensor showed good selectivity for Hg^{2+}.

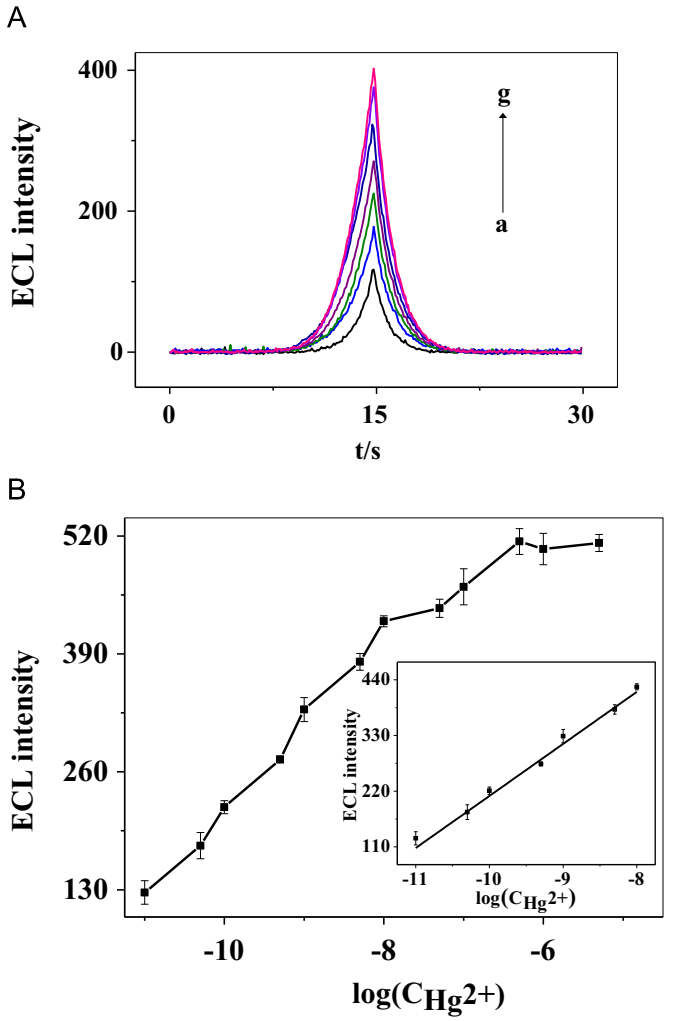

Fig. 4. (A) ECL intensity of the sensor exposed to different concentrations of Hg^{2+} (from bottom to top: 10^{-11}, 5×10^{-11}, 10^{-10}, 5×10^{-10}, 10^{-9}, 5×10^{-9}, and 10^{-8} mol/L). (B) Relationship between ECL intensity of the sensor and Hg^{2+} concentration. Inset is a logarithmic calibration curve for Hg^{2+}.

Fig. S3 illustrates the ECL of sensor during continuous CV scanning for 15 cycles in an electrolyte with an Hg^{2+} concentration of 10^{-7} mol/L. The ECL intensity of CdSe QDs/dsDNA/ERGO/GCE showed no apparent change during continuous CV scanning, demonstrating its good stability.

Table 1
Determination of Hg^{2+} in the Yongding River using the sensor.

Sample	Hg^{2+} added (nM)	Hg^{2+} concentration (mean ± SD) (nM)	Recovery (%)
Yongding River water	0	3.09 ± 0.12	
	2.00	5.17 ± 0.03	104
	5.00	7.99 ± 0.02	98

The reproducibility of the sensor was also evaluated. Six modified electrodes were used to detect Hg^{2+}. Furthermore, the sensor was stored in a refrigerator at 4 °C for 20 days and no obvious change of the response current was observed. These results indicate that the developed sensor has satisfactory reproducibility and stability.

3.7. *Detection of Hg^{2+} in a real water sample*

The prepared sensor was used to detect the concentration of Hg^{2+} in a real water sample obtained from Yongding River (Beijing, China). Prior to detection, the local river water was centrifuged to remove impurities, and then filtered through a 0.2-μm membrane. The water sample was measured by both the sensor and ICP-MS. Table 1 shows that the recovery of Hg(II) by the sensor was relatively high. The concentration of Hg^{2+} determined by the sensor was consistent with that obtained by ICP-MS (4.11×10^{-9} mol/L).

4. Conclusions

Aim to improve electron transfer performance in an electrochemical system, we fabricated a sensor based on the good conduction of graphene and facile charge transfer of dsDNA with T–Hg(II)–T base pairs. The ECL intensity was proportional to the logarithm of Hg^{2+} concentration within a certain range. Moreover, this ECL biosensor exhibit high sensitivity of detection Hg(II) in real water sample. The increased ECL intensity attributed to the formation of T–Hg(II)–T base pairs that accelerated the rate of charge transfer in dsDNA. Sensor based on high-intensity electron transfer interface will be a valuable approach to obtaining highly sensitive detection.

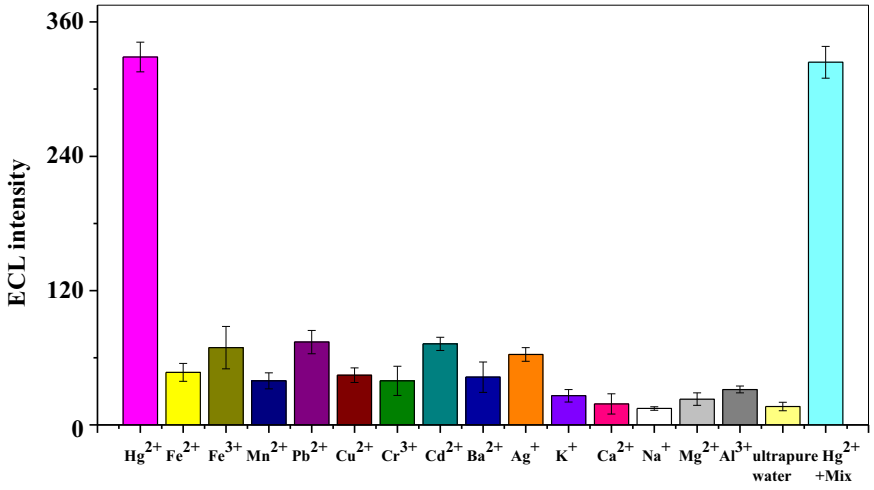

Fig. 5. Effect of interfering metal ions on the ECL signal response detected by the sensor. The bars represent 10^{-9} mol/L Hg^{2+}, 10^{-8} mol/L of other metal ions and a mixture of 10^{-9} mol/L Hg^{2+} and 10^{-8} mol/L each of the 14 other metal ions. Errors bars represent the standard deviation of three repeated experiments.

Acknowledgments

Thank for the support of Foundation of National Natural Science Foundation of China (Nos. 21005005, 21375005, and 21475006), Beijing Nova Program (No. 2010B009) and the Program for New Century Excellent Talents in University (NCET-12-0603).

Appendix A. Supplementary material

Supplementary data associated with this article can be found in the online version at http://dx.doi.org/10.1016/j.bios.2015.10.047.

References

Chen, L.Y., Tang, Y.H., Wang, K., Liu, C.B., Luo, S.L., 2011. Electrochem. Commun. 13, 133–137.
Dong, Z.M., Zhao, G.C., 2012. Sensors 12, 7080–7094.
Du, D.X., Guo, S., Tang, L.N., Ning, Y., Yao, Q.F., Zhang, G.J., 2013. Sens. Actuators B – Chem. 186, 563–570.
Escudero, L.B., Olsina, R.A., Wuilloud, R.G., 2013. Talanta 116, 133–140.
Filik, H., Cetintas, G., Avan, A.A., Koc, S.N., Boz, I., 2013. Int. J. Electrochem. Sci. 8, 5724–5737.
Gao, W.H., Zhang, A., Chen, Y.S., Chen, Z.X., Chen, Y.W., Lu, F.S., Chen, Z.G., 2013. Biosens. Bioelectron. 49, 139–145.
Guo, H.L., Wang, X.F., Qian, Q.Y., Wang, F.B., Xia, X.H., 2009. ACS Nano 3, 2653–2659.
George, G.N., Singh, S.P., Myers, G.J., Watson, G.E., Pickering, I.J., 2010. J. Biol. Inorg. Chem. 15, 709–715.
Huang, D.W., Niu, C.G., Ruan, M., Wang, X.Y., Zeng, G.M., Deng, C.H., 2013. Environ. Sci. Technol. 47, 4392–4398.
Jang, H., Kim, Y.K., Kwon, H.M., Yeo, W.S., Kim, D.E., Min, D.H., 2010. Angew. Chem. Int. Ed. 49, 5703–5707.
Jiang, H., Ju, H.X., 2007. Anal. Chem. 79, 6690–6696.
Jiang, W., Wang, W., 2009. Chem. Commun., 3913–3915.
Kratochviova, I., Golan, M., Vala, M., Sperova, M., Weiter, M., 2014. J. Phys. Chem. B. 118, 5374–5381.
Laviron, E., 1979. J. Electroanal. Chem. 101, 19–28.
Li, M., Wang, Q.Y., Shi, X.D., Hornak, L.A., Wu, N.Q., 2011. Anal. Chem. 83, 7061–7065.
Long, Y.T., Li, C.Z., Kraatz, H.B., Lee, J.S., 2003. Biophys. J. 84, 3218–3225.
Louie, H., Wong, C., Huang, Y.J., Fredrickson, S., 2012. Anal. Methods 4, 522–529.
Lu, C.H., Yang, H.H., Zhu, C.L., Chen, X., Chen, G.N., 2009. Angew. Chem. Int. Ed. 48, 4785–4787.
Ma, J., Chen, Y.H., Hou, Z., Jiang, W., Wang, L., 2013. Biosens. Bioelectron. 43, 84–87.
Miyake, Y., Togashi, H., Tashiro, M., Yamaguchi, H., Oda, S., Kudo, M., Tanaka, Y., Kondo, Y., Sawa, R., Fujimoto, T., Machinami, T., Ono, A., 2006. J. Am. Chem. Soc. 128, 2172–2173.
Niu, X.H., Ding, Y.L., Chen, C., Zhao, H.L., Lan, M.B., 2011. Sens. Actuators B – Chem. 158, 383–387.
Pheeney, C.G., Barton, J.K., 2013. J. Am. Chem. Soc. 135, 14944–14947.
Reis, A.T., Lopes, C.B., Davidson, C.M., Duarte, A.C., Pereira, E., 2014. Geoderma 213, 255–260.
Shao, Y.Y., Wang, J., Engelhard, M., Wang, C.M., Lin, Y.H., 2010. J. Mater. Chem. 20, 743–748.
Stanisavljevic, M., Janu, L., Smerkova, K., Krizkova, S., Pizurova, N., Ryvolova, M., Adam, V., Hubalek, J., Kizek, R., 2013. Chromatographia 76, 335–343.
Steel, A.B., Herne, T.M., Tarlov, M.J., 1998. Anal. Chem. 70, 4670–4677.
Tan, H.L., Zhang, Y.Q., Chen, Y., 2011. Sens. Actuators B – Chem. 156, 120–125.
Wang, L.L., Yao, T.M., Shi, S., Cao, Y.L., Sun, W.L., 2014. Sci. Rep. 4, 5320.
Wang, Y.L., Zhao, G.C., 2011. Int. J. Electrochem. 2011, 1–6.
Xu, E.S., Lv, Y.Q., Liu, J.F., Gu, X.H., Zhang, S.Q., 2015. RSC Adv. 5, 49819–49823.
Yang, T., Li, Q.H., Meng, L., Wang, X.H., Chen, W.W., Jiao, K., 2013. ACS Appl. Mater. Interfaces 5, 3495–3499.
Yu, H.Z., Luo, C.Y., Sankar, C.G., Sen, D., 2003. Anal. Chem. 75, 3902–3907.
Zhang, B.T., Guo, L.H., 2012. Biosens. Bioelectron. 37, 112–115.
Zhang, Y., Zhao, H., Wu, Z.J., Xue, Y., Zhang, X.F., He, Y.J., Li, X.J., Yuan, Z.B., 2013. Biosens. Bioelectron. 48, 180–187.
Zhao, Z., Zhou, X.M., 2012. Sens. Actuators B–Chem 171–172, 860–865.
Zhou, M., Wang, Y.L., Zhai, Y.M., Zhai, J.F., Ren, W., Wang, F., Dong, S.J., 2009. Chem. Eur. J. 15, 6116–6120.